REPORT DOCUMENTATION PAGE

Form Approved
OMB No. 0704-0188

1. REPORT DATE *(DD-MM-YYYY)*	2. REPORT TYPE	3. DATES COVERED *(From - To)*
01-05-2010	Final	April 15, 2007-May 1, 2010

4. TITLE AND SUBTITLE
Investigation of Ferromagnetic Semiconductor Devices for Spintronics

5a. CONTRACT NUMBER

5b. GRANT NUMBER
FA9550-07-1-0381

5c. PROGRAM ELEMENT NUMBER

6. AUTHOR(S)
Bruce Wessels

5d. PROJECT NUMBER

5e. TASK NUMBER

5f. WORK UNIT NUMBER

7. PERFORMING ORGANIZATION NAME(S) AND ADDRESS(ES)
Northwestern University, 633 Clark Street, Evanston, IL 60208

8. PERFORMING ORGANIZATION REPORT NUMBER

9. SPONSORING/MONITORING AGENCY NAME(S) AND ADDRESS(ES)
AF Office of Scientific Research
875 N. Randolph St., Room 3112
Arlington, VA 22203-1954

10. SPONSOR/MONITOR'S ACRONYM(S)
USAF, AFRL

11. SPONSORING/MONITORING AGENCY REPORT NUMBER

12. DISTRIBUTION AVAILABILITY STATEMENT
Approved for Public Release; Distribution is Unlimited

13. SUPPLEMENTARY NOTES

14. ABSTRACT
Spintronic devices are being developed as an alternative to conventional semiconductor devices for many applications including information storage, communications and information processing. Hybrid unipolar devices comprising ferromagnetic metals and semiconductors have been employed to demonstrate spin injection and detection in Si. However, for integration and fabrication of all-semiconductor magnetoelectronic devices, dilute magnetic semiconductors (DMS) are the most likely candidates, and many possible unipolar and bipolar devices have been already proposed using these materials. In particular the bipolar magnetic junction transistor (MJT) has been predicted to have unique properties like magneto-amplification (MA), which is the change of amplification upon application of an external magnetic field. Here we report on the room-temperature operation of a InMnAs based bipolar magnetic junction transistor. Magnetoamplification is observed for the first time in a bipolar magnetic junction transistor.

15. SUBJECT TERMS
Magnetic III-V semiconductors, bipolar magnetic junction transistors

16. SECURITY CLASSIFICATION OF:			17. LIMITATION OF ABSTRACT	18. NUMBER OF PAGES	19a. NAME OF RESPONSIBLE PERSON
Unclassified			UU	25	Bruce Wessels
a. REPORT	b. ABSTRACT	c. THIS PAGE			19b. TELEPONE NUMBER (*Include area code*) 847-491-3219

1. Background for InMnAs magnetoresistance

Recent years have witnessed intense activity aimed at developing semiconductors that enable combining both the electronic charge and the spin degree of freedom into a single magnetoelectronic device. The novelty of such ”spintronic" devices lies in manipulating the spin states of the mobile carriers while maintaining their charge functionality in electronic data processing. In this regard, III-Mn-V dilute magnetic semiconductors (DMS) are promising candidates for such applications with the Mn^{2+} ions providing both localized magnetic moments and valence band holes. Of particular interest are nominally single phase $In_{1-x}Mn_xAs$ thin films (with $x<0.10$) grown by metal-organic vapor phase epitaxy (MOVPE). These thin films have been found to be ferromagnetic up to 330 K, indicating their potential in various spintronic applications at room temperature.

The assessment of magnetic characteristics by means of magneto-transport measurements is very useful in the case of thin films of diluted magnetic semiconductors, in which the magnitude of the magnetization is typically small. The presence of local magnetic moments and, in particular, the exchange interaction between carriers and local moments has been known to dramatically modify carrier transport. As a result of this exchange interaction, there is a giant spin splitting of electronic bands and a resultant shift of the metal-insulator transition to higher carrier concentrations. Several theoretical models have been proposed that describe the origins of the magnetoresistance in these materials. A theory of spin-disorder scattering by thermodynamic fluctuations of magnetic atoms has been developed for ordered magnetic semiconductors based on an earlier theory of scattering in magnetic metals. It was shown that the application of an external magnetic field decreases the thermodynamic fluctuations of the local magnetization (due to atomic moments of the magnetic ions) and leads to negative magnetoresistance. Positive magnetoresistance on the other hand has been recently attributed to increased scattering of carriers from localized magnetic moments due to a local increase in the magnitude of the band splitting as a result of the Zeeman Effect. The enhancement of spin-dependent scattering by the external magnetic field is especially large for semiconductors with electrically active magnetic impurities. Alternatively the positive magnetoresistance has been attributed to conduction via two bands with different conductivities and mobilities.

Low-field magnetoresistive properties of InMnAs thin films have been previously measured up to 14 K, revealing a negative magnetoresistance behavior that was attributed to spin-selective scattering in an impurity band and described by the Khosla-Fisher magnetotransport model for negative magnetoresistance. At temperatures above 14 K a small positive magnetoresistance was observed, however the mechanism responsible for the behavior was not identified. Temperature dependent resistivity and Hall Effect measurements confirmed the existence of low temperature impurity band conduction in this material.

In contrast to the low temperature magnetoresistance of InMnAs thin films, subsequent studies of the transport properties of InMnAs/InAs p-n junctions revealed a saturating giant positive magnetoresistance in the presence of a longitudinal magnetic field. The magnetoresistance of the p-n junction was measured in magnetic fields of up to 18 T over the temperature range of 80-300 K and was found to exceed 2600% at 300 K. The giant positive magnetoresistance was subsequently attributed to conduction of spin-polarized carriers due to the presence of spin-split bands.

In the present work we measured the magnetotransport properties of MOVPE-grown $In_{0.95}Mn_{0.05}As$ over the temperature range of 19 - 61 K and in magnetic fields of up to 1 T. Contrary to prior low temperature measurements that show a negative magnetoresistance for InMnAs, a predominantly positive magnetoresistance is observed above 17 K with only a small negative component. The data supports a semi-empirical model for the magnetotransport of carriers in diluted magnetic semiconductors that takes into account the third order *p-d* exchange Hamiltonian to describe the negative contribution and a two band model involving spin-split bands for the positive contribution.

2. Magnetoresistance Model

To explain the magnetoresistive properties of $In_{0.95}Mn_{0.05}As$ thin films, we have used a model that takes into account both the negative and positive contributions to the magnetoresistance. The presence of negative magnetoresistance is usually understood as the result of localized magnetic moment scattering, originally proposed by Toyozawa. According to this model, carriers are scattered by localized magnetic moments of the magnetic impurity atoms. The application of an external magnetic field orders these magnetic moments and reduces scattering, resulting in a decrease in resistivity. However, Khosla and Fischer argued that while the qualitative features of the negative magnetoresistance at low fields were consistent with the

localized magnetic moment model of Toyozawa, there were quantitative disagreements with the calculations based on the second-order perturbation expansion of the exchange Hamiltonian. They thus suggested that third order terms in the expansion be included and a semi-empirical expression for the negative magnetoresistance was derived with the form:

$$\frac{\Delta\rho}{\rho} = -B_1^2 \ln(1 + B_2^2 H^2) \quad (1),$$

The model proposed in Eqn. (1) can be used to describe negative magnetoresistance for other degenerate semiconductors. The parameters B_1 and B_2 are given by:

$$B_1 = A_1 J \rho_F [S(S+1) + < M^2 >] \quad (2),$$

and

$$B_2^2 = \left[1 + 4S^2\pi^2\left(\frac{2J\rho_F}{g}\right)^4\right]\left(\frac{g\mu_B}{\alpha k_B T}\right)^2 \quad (3),$$

where J is the exchange interaction energy, g is the Lande factor, ρ_F is the density of states at the Fermi energy, $<M^2>$ is the average magnetization of the localized paramagnetic ions squared, S is the spin of the localized magnetic moment, and α is a numerical constant ranging from 0.1 to 10. The parameter A_1 is regarded to be a measure of contribution of spin scattering to the total magnetoresistance. The magnitude of the negative magnetoresistance given by Eq. 1. decreases with an increase in carrier concentration and temperature.

To explain the origin of the positive magnetoresistance, a two-band model has been proposed for magnetic semiconductors. In this model, the classical positive magnetoresistance arises from the action of the Lorentz force on mobile carriers in two bands. The two-band model for the magnetic field dependence of electrical resistance of metals was first introduced by Sondheimer and Wilson where they considered conduction via one composite conduction band, consisting of overlapping partially filled *s*- and *d*-bands. Analyses based on such a model show that the positive magnetoresistance is given by:

$$\frac{\Delta\rho}{\rho} = \frac{B_3^2 H^2}{\left(1 + B_4^2 H^2\right)} \quad (4),$$

where the parameters

$$B_3 = \frac{\sigma_1\sigma_2(\mu_1+\mu_2)^2}{(\sigma_1+\sigma_2)^2} \quad (5),$$

and

$$B_4 = \frac{(\sigma_1\mu_2-\sigma_2\mu_1)^2}{(\sigma_1+\sigma_2)^2}, \quad (6),$$

are the conductivity σ_i and mobility μ_i of carriers in the two bands. The magnetoresistance described by Eqn. (4) is quadratic at low fields, and saturates at high fields.

As to the nature of the two band model and its relevance to DMS it has been applied to ZnO and ZnCoO. In these studies two bands were used to model the Hall coefficient and magnetoresistance. In the present study we attribute the two bands to a hybridized *p*-*d* band (*p*-valence band and *d*-impurity band) that is spin-split due to the giant Zeeman effect. Two bands form consisting of spin-polarized carriers with different conductivity and mobility (see figure 1). It is well known that in DMS, kinetic mixing of the *p*- and *d*-bands due to the hybridization of their wavefunctions results in a giant Zeeman splitting of the band structure when an external magnetic field is applied. Furthermore, it has been shown theoretically that the Zeeman spin-splitting can play a very important role in the magnetoresistance of DMS. Consequently, it was shown for GaMnAs and ZnMnO that the Zeeman spin-splitting of the band states results in a positive magnetoresistance.

We thus propose that two magnetotransport mechanisms are responsible for the magnetoresistance behavior of the $In_{1-x}Mn_xAs$ film under investigation – spin-dependent scattering by localized magnetic moments results in a negative magnetoresistance and a magnetic field-induced change in the conductivities of the two spin-split hybridized *p*-*d* bands yields a positive magnetoresistance. The field dependence of the observed transverse magnetoresistance can be described by adding the negative and positive contributions. By combining Eqns. 1 and 4 the magnetoresistance is given by:

$$\frac{\Delta\rho}{\rho} = -B_1^2\ln(1+B_2^2H^2) + \frac{B_3^2H^2}{(1+B_4^2H^2)}, \quad (7)$$

3. Experiment

The $In_{1-x}Mn_xAs$ film was epitaxially deposited on a semi-insulating GaAs (001) substrate using atmospheric pressure MOVPE at 520°C. InMnAs grown by this technique has a T_c of 330

K. Energy dispersive X-ray spectroscopy was used to determine the Mn concentration (x=0.05) in the film. Details of the growth procedure are reported elsewhere. Extensive X-ray and TEM measurements indicate the films are phase pure within the detection limits of these techniques. Evidence of ferromagnetic ordering in $In_{1-x}Mn_xAs$ films grown by MOVPE has been reported elsewhere.

The samples for magnetotransport measurements were prepared using standard fabrication techniques of conventional photolithography and wet chemical etching to pattern the film into a Hall bar configuration. The film thickness was 500 nm. Ohmic contacts were made by soldering dots of indium on the contact pads of the Hall bar and gold wires were used to make electrical leads to the device. Hall Effect measurements were performed over the temperature range of 5 to 300 K under applied magnetic fields of up to 1 T. A nominal hole concentration of $1x10^{18}$ cm^{-3} at 295 K was obtained from Hall Effect measurements. To determine the transverse magnetoresistance, the resistivity of the film was measured with the magnetic field applied perpendicular to the plane of the film. The zero-field resistivity was found to be 1 ohm-cm at 5 K and 0.04 ohm-cm at 300K.

4. Magnetoresistance Results and Discussion

The magnetoresistance of the InMnAs was measured in magnetic fields up to 1 Tesla. Plots of magnetoresistance versus magnetic field at four different temperatures (19, 33, 47, and 61 K) are shown in figure 2. We see from the graph that in the low-field region the magnetoresistance is initially negative and only becomes positive as the field increases. Given that the sample shows both negative and positive contributions to the magnetoresistance, least-squares fits to the data were performed using Eq. (7). Representative fits, indicated by the solid lines through the data points, are shown in figure 2 for the four different temperatures. At low fields and temperatures the first term of Eq. (7) predominates and negative magnetoresistance is observed. At higher fields the second term dominates and a positive magnetoresistance is observed. The values of the fitting parameters B_1, B_2, B_3, and B_4 for each temperature are given in Table I.

The parameters B_1 and B_2, which describe the negative magnetoresistance are temperature dependent as shown in Table 1. Specifically, values of B_2 obtained from the fitting of the data to Eq. (7) are nearly linear with 1/T, in agreement with the predications of the theory

in Eqn. (3).. As observed in figure 2, at low fields and for temperatures below 61 K, the negative component increases in strength with decreasing temperature consistent with Eq. (3). Since the coefficients B_1 and B_2 are functions of various parameters such as exchange interaction, spin-splitting factors, and other numerical constants [Eqs. (2) and (3)], which are unknown in the case of MOVPE-grown InMnAs thin films, no further analysis of these coefficients were made.

We also observe from figure 2 that the mechanism that results in the negative magnetoresistance competes with that which produces the positive component, with the latter dominating at higher temperatures and fields. The small negative component is caused by reduced scattering due to the spin alignment of the local magnetic moments in the impurity band. At higher temperatures spin-ordering is strongly suppressed and the positive component dominates; this is evident in the diminishing strength of the negative magnetoresistance between 19 K and 61 K and also in the decrease in the value of B_2 over the same temperature range (Table 1). The magnitude of the positive magnetoresistance observed in figure 2 is a function of B_3 and B_4 as derived in Eqns. (5) and (6). These parameters are related to the conductivities and carrier mobilities in the two spin sub-bands. As indicated the positive magnetoresistance is described by a model in which the hybridized *p-d* band in the thin film is spin-split due to the giant Zeeman effect, forming two bands consisting of spin-up and spin-down carriers (Fig. 1). The magnetic field splitting of the band, and the resulting changes in the density of states, result in different populations of the two spin sub-bands with different conductivity and mobility for majority and minority spin carriers, respectively. Increased scattering of spin-polarized carriers due to a local increase in the magnitude of the band splitting as a result of the Zeeman effect leads to the positive magnetoresistance.

It is noted in Table 1 that the values of the parameters B_3 and B_4 decrease with increasing temperature. The difference in the mobilities of the spin-spilt bands is attributed to different scattering times for the spin-polarized carriers. At low temperatures the conductivity increases presumably due to reduced phonon scattering of carriers; this results in longer scattering times and hence larger mobility values. Hence the variation of the coefficients B_3 and B_4 with temperature shown in Table 1 is reasonable. Furthermore this behavior has also been observed in other degenerate semiconductor systems. Values of B_3 and B_4 were also calculated above 0.3 T using only Eqn. (4), thereby neglecting effects of the negative magnetoresistance. It was found that the values of B_3 and B_4 using either Eqn. 4 or Eqn. (7) were comparable. The change in

magnetoresistance calculated using the two-band model of Eqn. (4) is proportional to H^2 for small fields and reaches a constant value for very large fields. This low field behavior is confirmed as shown in Figure 3 where the magnetoresistance curves follow similar quadratic field dependence at low magnetic fields.

For comparison, only a weak negative MR was observed for LT MBE InMnAs. The MR was attributed to scattering by magnetic polarons.

5. Magnetoamplification in a bipolar magnetic junction transistor

The basic building blocks of a bipolar magnetic junction transistor are magnetic diodes. Recently, we have shown that p-n junctions using the p-type magnetic semiconductor InMnAs show a giant positive magnetoresistance. The magnetotransport properties of InMnAs/InAs p-n junctions were previously simulated using a modified Shockley equation that includes magnetoresistive effects. The giant positive magnetoresistance is attributed to spin-selective conduction through spin split bands. InMnAs when grown by metal organic vapor phase epitaxy (MOVPE) is a ferromagnetic semiconductor with a Curie temperature of 330K. Magnetic circular dichroism experiments on InMnAs indicate strong s,p-d exchange at room temperature leading to formation of spin-split bands that results in a positive magnetoresistance. The giant magnetoresistive properties of the InMnAs junction make this material an ideal candidate for use in an MJT.

6. Device fabrication and testing:

Figure 4 shows the device structure of the InMnAs bipolar MJT used in this study. P-type InAs ($p_E = 5\times10^{18}cm^{-3}$) substrate is the emitter and the InMnAs ($p_C = 1\times10^{18}cm^{-3}$) epitaxial layer is the collector. A 150nm thick layer of undoped epitaxial layer of InAs serves as the base. The InMnAs/InAs/p-InAs heterojunctions were fabricated by depositing 150 nm of InAs ($n_B = 1\times10^{16}cm^{-3}$) by metalorganic vapour phase epitaxy followed by 75nm of InMnAs on p-type (001) InAs substrate. Photolithography was used to define circular Ti/Au collector contacts with a 250 μm diameter. The base and emitter contacts were defined in subsequent photolithography and contact deposition steps.

The transistor properties were measured using a Keithley 4200 semiconductor parametric analyzer. All reported measurements are in the common emitter mode where the InAs p-type substrate serves as the emitter. The I-V characteristics were measured at 298K. The emitter-

collector voltage is varied between 0 to 0.4V, and the base current ranges from 0 to 5μA, in steps of 1μA . The transistor characteristics were measured in a magnetic field that is perpendicular to the plane of the junction, using fields from 0 to 8 T.

7. Transistor model

To explain the behavior of a bipolar magnetic junction transistor in the presence of a magnetic field, its characteristics have been previously modeled for the case of a magnetic emitter and base. An Ebers-Moll transistor model was used and these calculations showed that in the presence of an equilibrium spin polarization, injection and transport of spin polarized carriers leads to a change of amplification for the transistor with magnetic field strength. Furthermore, additional changes in the amplification can be achieved by the injection of spin-polarized carriers from an external source. In this model, the equilibrium spin (due to spin splitting of the conduction or valence band of the semiconductor) is accounted for in the pre-factor to the forward and reverse biased coupled diode current expressions. The model predicts a positive magneto-amplification effect where increasing the magnetic field leads to an increase in amplification.

In contrast, a negative magneto-amplification was observed where increasing the magnetic field leads to a decrease in amplification. To describe the experimentally observed transistor characteristics, we propose a modified Ebers-Moll equivalent circuit that includes a series magnetoresistance. In the absence of non-equilibrium spin, the reverse current term used in the Ebers-Moll model for a bipolar magnetic junction transistor is replaced with a modified Shockley diode equation. Figure 5 shows the equivalent circuit for the device consisting of two coupled diodes and a magnetic field dependent resistance R(B) in series with the collector-base (reverse) diode. This resistance accounts for the magnetoresistance in the collector base magnetic junction. The modified reverse diode current (I_R) is given by:

$$I_R = I_{R0}\exp\left(\frac{V_{CB} - I_R R(B)}{\eta_{CB} Vt}\right) \quad \text{……..……(8)}$$

where I_{R0} is the current pre-factor, $R(B)$ is the magnetic-field dependent resistance, η_{CB} is the junction ideality factor, Vt is the thermal voltage, and V_{CB} is the applied bias .The details of the model are given in the supplemental information.

The modified Ebers-Moll model is used to relate the magneto-amplification of the transistor to the magnetoresistance of the collector-base junction. The magneto-amplification results from the magnetoresistance of the collector-base (p-InMnAs/undoped-InAs) junction. We attribute the magnetoresistance in the collector-base junction to spin-dependent transport through two spin channels. When a magnetic field is applied, spin-selective transport in the reverse biased p-n junction leads to an increase in R(B) as has been previously shown. This in turn leads to a decrease in the collector current both for a zero base current and finite base current. Since the decrease in the collector current for a finite base current is larger than the decrease in the collector current at zero base current, this leads to a negative magneto-amplification. For a given emitter collector bias (V_{EC}) and given base current I_B, a change in the resistance in InMnAs/InAs junction results in changes in both the forward and reverse diode currents as these diodes are coupled. Our calculations show that the magneto-amplification depends on the functional form of the magnetoresistance for the InMnAs collector junction and its magnetic field dependence. Furthermore, our calculations show that for a given base current the magneto-amplification decreases for increasing V_{EC} .

8. Transistor characteristics

Figure 6 shows the measured characteristics of the bipolar MJT where the magnetic InMnAs layer is the collector. The device shows tendency towards saturation for voltages less than 0.05V. For voltages higher than 0.05V, the slope of the collector current curve decreases as expected for the active region of a transistor. With an increase in base current, an increase in the collector current is observed as shown in the inset. As V_{EC} is increased, there is a corresponding increase in the collector current. This presumably results from base width modulation (Early effect) and leads to a non-zero slope. A reverse bias applied to the n-InAs/p-InMnAs junction results in a very high hole current that leads to the high collector currents observed in the transistor. The high hole concentration of $5\times10^{18}cm^{-3}$ in the p-InAs emitter improves the transistor performance. At higher V_{EC}, an increase in slope occurs in the collector current curve.

Small changes in the base current result in significant changes in the collector current and correspond to a positive amplification. The amplification (β_{dc}) of the transistor was measured where β_{dc} is defined as follows:

$$\beta_{dc} = \frac{I_C(I_B) - I_C(0)}{I_B} \qquad \text{……..(9)}$$

where $I_C(I_B)$ is the collector current for a constant base current of (I_B) and $I_C(0)$ is the collector current for zero base current.

In Figure 7 the amplification is plotted as a function of the collector current on a log-log plot for different base current values. The highest amplification observed for our heterojunction device is 20. For comparison, much higher amplifications (as high as 400) have been achieved in InAs homojunction transistors grown by MBE when a optimized carrier concentration profile that decreases collector current is used. In the MJT, for a very low collector current the amplification is very small due to generation-recombination in the emitter-base depletion region. As the collector current increases the relative contribution of generation-recombination current to the total collector current decreases thereby leading to an increase in the amplification of the device. For a low collector current, the amplification is a function of the collector current given by $\beta_{dc} \propto I_C^{\left(1-\frac{1}{\eta_{EB}}\right)}$ where η_{EB} is the ideality factor for the emitter base junction. Thus, on a log-log plot, the relationship between the log of amplification and log of collector current is linear, as is evident in Figure 7 for a base current of 2 μA.

At intermediate collector currents, there is a narrow region where the transistor characteristics approach ideal behavior, and a plateau is reached in the amplification-collector current curve. However, at higher collector currents the amplification drops rapidly. Note that the slope of the amplification curve is larger (and negative) in the high collector current region. In this case, an increase in the base or emitter resistance leads to a decrease in the collector current and amplification. A high injection level caused by current crowding also adds to a decreasing amplification at higher voltages. This is a result of deviation of the emitter base junction from ideal diode behavior.

In the presence of an external magnetic field, a change in the device amplification is observed. The change in amplification upon application of an external magnetic field, the magneto-amplification (MA), is calculated as follows:

$$MA = \frac{\beta_{dc}(B) - \beta_{dc}(0)}{\beta_{dc}(0)} \times 100 \qquad \text{……(10)}$$

where the term $\beta_{dc}(B)$ is the amplification at a magnetic field of B and a bias V_{EC}, and $\beta_{dc}(0)$ is the zero magnetic field amplification at the same bias. The magneto-amplification is calculated

for a constant emitter-collector bias for a given base current. For the case of $\beta_{dc}(B) < \beta_{dc}(0)$ a negative magneto-amplification results.

Figure 8 shows the magneto-amplification as a function of magnetic field and emitter-collector bias. A negative magneto-amplification is observed for magnetic fields between zero and 8T and voltages between 0.18V and 0.30V. For magnetic fields of less than 2T, the absolute magneto-amplification rises rapidly with field whereas for fields higher than 2T, the decrease in amplification with field is smaller. As V_{EC} is further increased, the absolute magnitude of magneto-amplification subsequently decreases. For voltages higher than 0.03 V but less than 0.18V, the absolute magneto-amplification is much higher since the device is not in saturation. This bias dependence of magneto-amplification indicates that the region for active operation decreases with increasing magnetic field.

The observed negative magneto-amplification qualitatively agrees with calculations using the modified Ebers-Moll equations. For a given magnetic field, the calculated magneto-amplification decreases with increasing emitter-collector bias. The non-idealities in the junction that lead to the very high currents are neglected in the model. This results in the quantitative differences between the experimental data and the calculated magneto-amplification.

The magneto-amplification curve is similar to the magneto-current dependence of magnetic field for a InMnAs/InAs diode. The sudden increase in magneto-amplification at lower magnetic fields and the gradual saturation is similar in functional form for the previously experimentally observed magneto-current ratio for magnetic semiconductor junctions.

As can be seen in Fig 7, one could in principle turn a transistor from an amplifying “on” state to a non-amplifying “off” state by changing the magnitude of the a magnetic field. This presumably could be achieved while the device is in operation and could potentially lead to reconfigurable logic. This magnetic control over the amplification could potentially result in applications in new paradigms of computer architecture.

Summary

In summary, low-field magnetotransport on MOVPE-grown $In_{0.95}Mn_{0.05}As$ magnetic has been measured over the temperature range of 19 – 61 K. The results of the temperature dependent magnetoresistance measurements are well described by the Khosla-Fischer model magnetotransport model for semiconductors with localized magnetic moments. At low fields and temperature the film exhibits negative magnetoresistance. Above 17 K the positive

magnetoresistance component predominates even at low fields. The positive magnetoresistance is best described using a two-band conduction model where the bands consist of spin-split hybridized *p-d* sub-bands with different mobilities. Application of a magnetic field induces a change in the relative populations of these spin sub-bands and results in the observed positive quadratic dependence of magnetoresistance on field.

We have demonstrated the first bipolar MJT using a magnetic semiconductor. For a InMnAs pnp transistor room temperature magneto-amplification is observed that depends on the base current and the emitter-collector bias. The observed magneto-amplification is attributed to the positive magnetoresistance of the magnetic semiconductor InMnAs heterojunction. The magnetic field dependence of the transistor characteristics confirms that the magneto-amplification results from the magnetoresistance of the collector junction. The capability of magnetic field control of the amplification in an all semiconductor transistor at room temperature potentially enables the creation of new computer logic architecture where the spin of the carriers is utilized.

Publications supported by this contract

"Giant magnetoresistance of magnetic semiconductor heterojunctions," with N. Rangaraju, Pengcheng Li, and B.W. Wessels, Phys. Rev. B, **79** 20, 205209 (2009).

"Magnetoresistance of InMnAs magnetic semiconductors," with J.A. Peters and B.W. Wessels, Physica E **42** 1497 (2010).

"Magnetotransport properties of InMnSb magnetic semiconductor thin films" with J.A. Peters, N. D. Parashar, N. Rangaraju and B.W. Wessels, PRB (2010) submitted.

"Magnetotransport in InMnAs based bipolar magnetic junction transistor," N. Rangaraju, J. A. Peters and B.W. Wessels, submitted

Patent disclosure

Magnetic semiconductor bipolar transistors, May 2010

Personnel

B. W. Wessels, PI, N. Rangaraju, Doctoral student, J. A. Peters, Post-doctoral fellow, P. Li, Post-doctoral fellow.

List of Figures

Figure 1

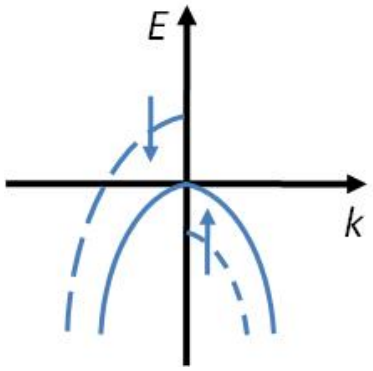

Figure 2

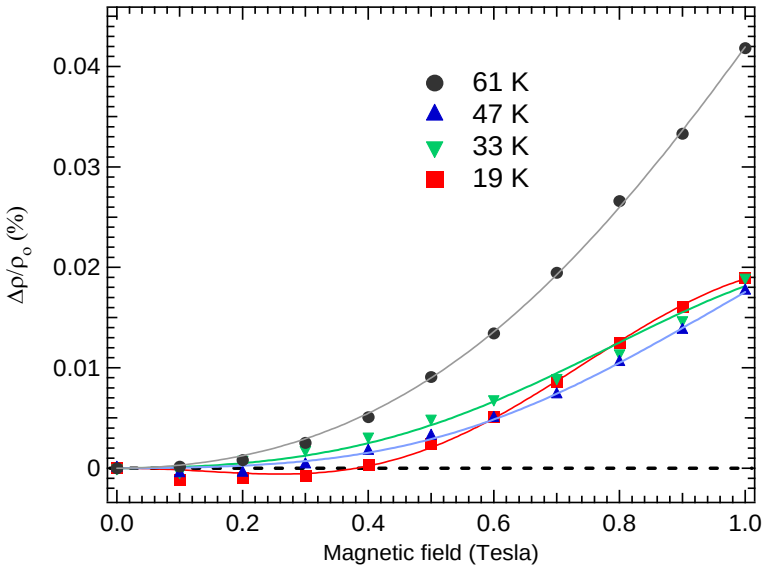
61 K
47 K
33 K
19 K
Δρ/ρo (%)
0.04
0.03
0.02
0.01
0
0.0
0.2
0.4
0.6
0.8
1.0
Magnetic field (Tesla)

Figure 3

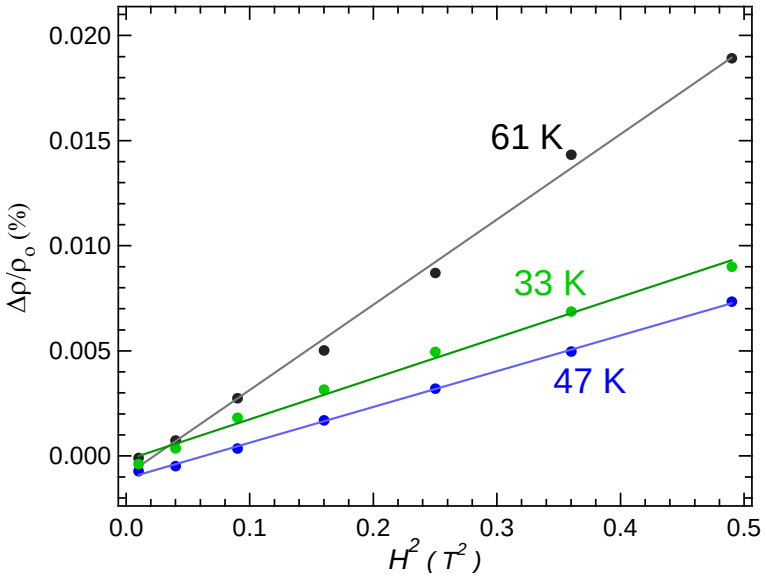

Figure 4

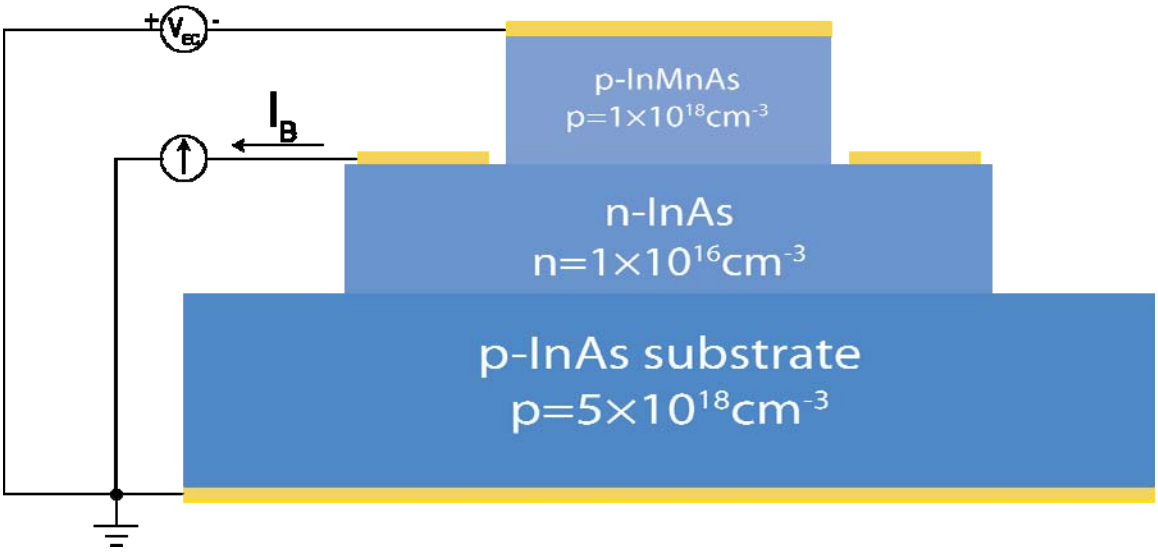
+
V_{EC}
-
I_B
p-InMnAs
p=1×10¹⁸cm⁻³
n-InAs
n=1×10¹⁶cm⁻³
p-InAs substrate
p=5×10¹⁸cm⁻³

Figure 5

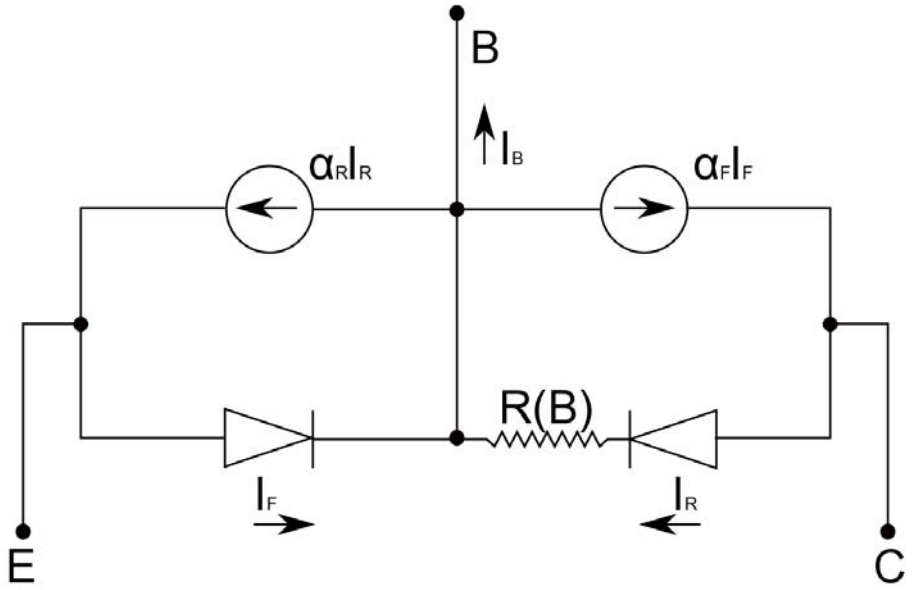

Figure 6

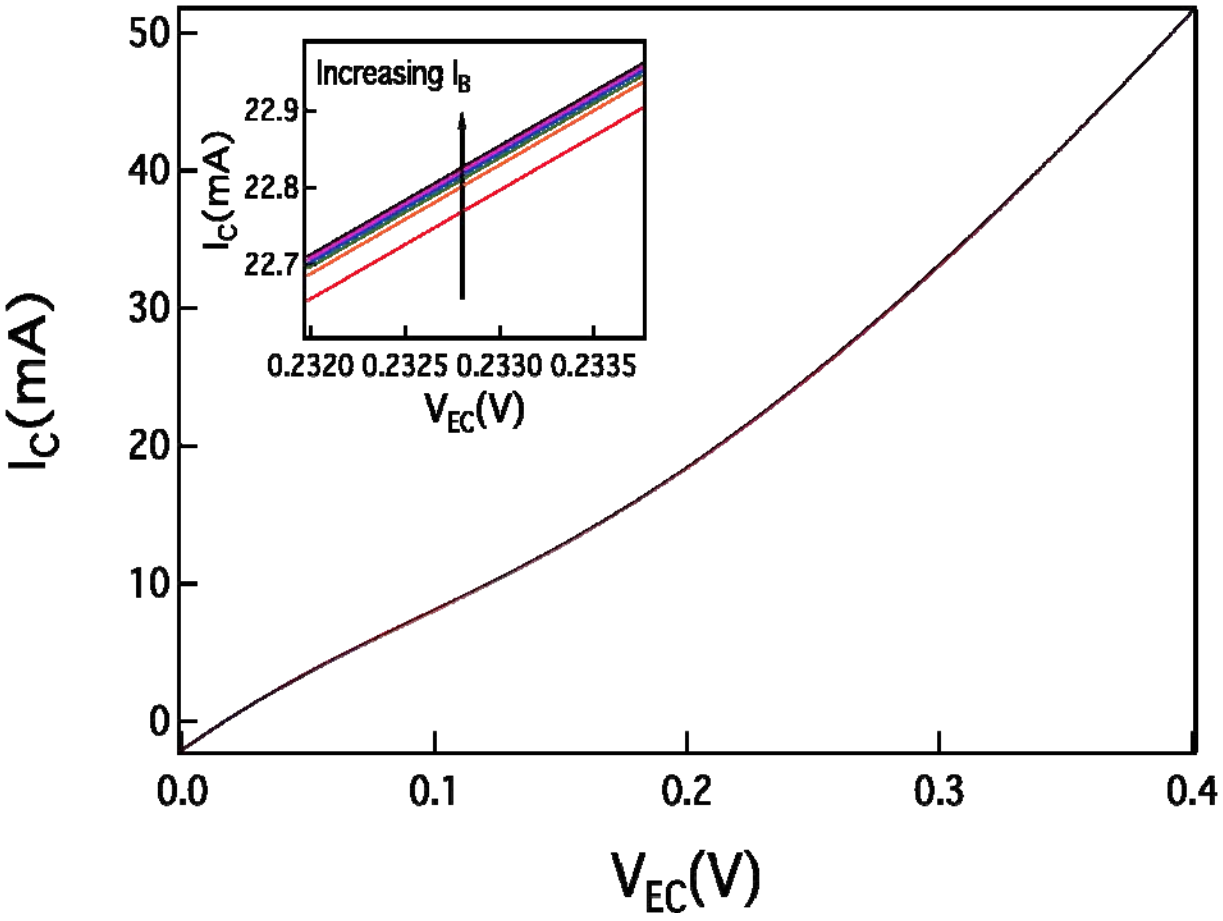
Increasing I_B
I_C(mA)
22.9
22.8
22.7
0.2320 0.2325 0.2330 0.2335
V_{EC}(V)
I_C(mA)
50
40
30
20
10
0
0.0
0.1
0.2
0.3
0.4
V_{EC}(V)

Figure 7

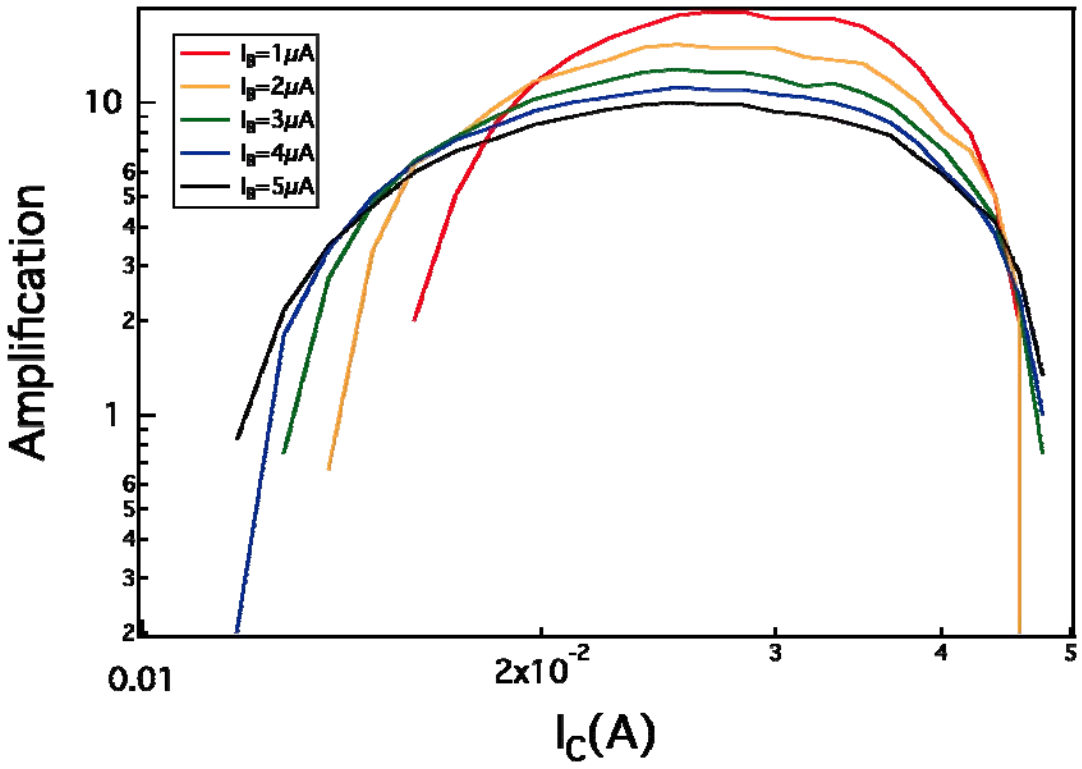
I_B=1μA
I_B=2μA
I_B=3μA
I_B=4μA
I_B=5μA
Amplification
10
6
5
4
3
2
1
6
5
4
3
2
0.01
2x10^{-2}
3
4
5
I_C(A)

Figure 8

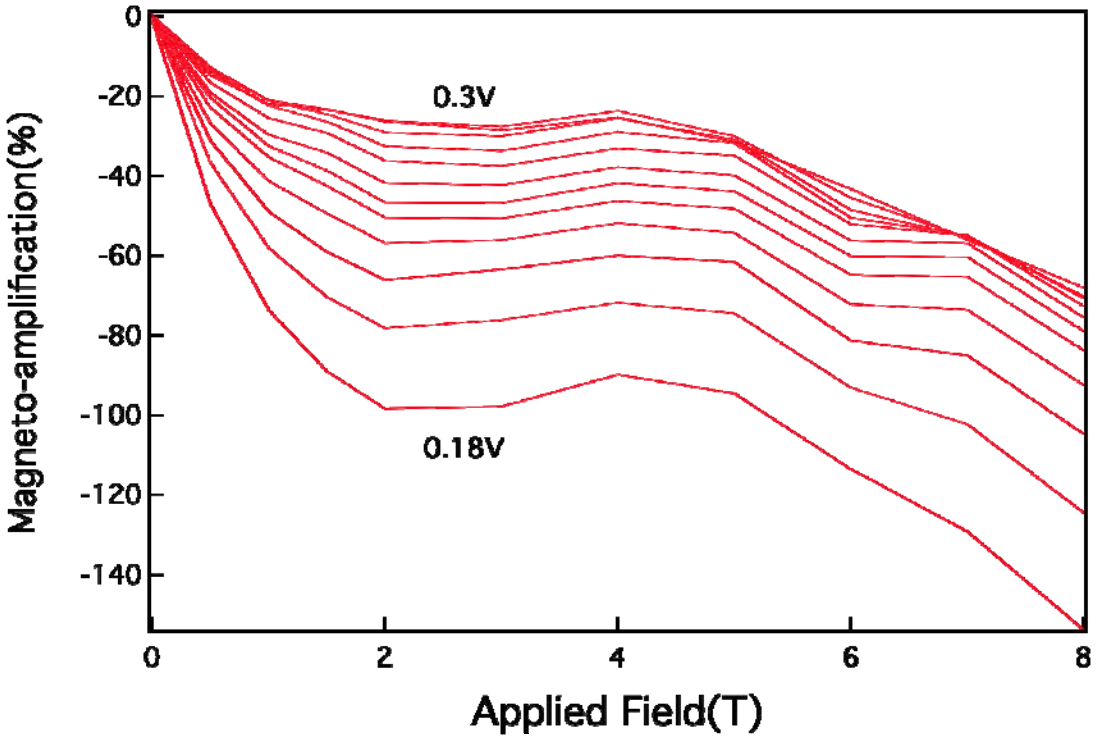
0
-20
-40
-60
-80
-100
-120
-140
Magneto-amplification(%)
0.3V
0.18V
0
2
4
6
8
Applied Field(T)

TABLE I. Values of the fitting parameters to the Eq. 7.

T (K)	B_1	B_2 (T^{-1})	B_3	B_4
19	0.857 ± 0.0011	1.138 ± 0.0006	0.966 ± 0.0010	0.695 ± 0.0004
33	1.051 ± 0.0010	0.828 ± 0.0011	0.915 ± 0.0003	0.551 ± 0.00006
47	1.083 ± 0.0021	0.765 ± 0.0009	0.814 ± 0.0001	0.507 ± 0.0023
61	1.105 ± 0.0016	0.741 ± 0.0005	0.796 ± 0.0006	0.493 ± 0.00008